Marine Geology 470 (2024) 107250

Contents lists available at ScienceDirect

Marine Geology

journal homepage: www.elsevier.com/locate/margo

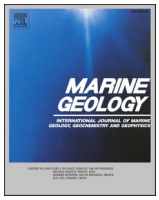

Manganese diagenesis in different geochemical environments of the ria de Vigo (Galicia, NW Iberian Peninsula)

X.L. Otero [a,b,*], A.M. Ramírez-Pérez [c], M. Abernathy [d], S.C. Ying [e], H.M. Queiroz [h], T.O. Ferreira [f], M.A. Huerta-Díaz [g], E. de Blas [c]

[a] CRETUS. Dpto. Edafoloxía e Química Agrícola, Universidade de Santiago de Compostela, 15782 Santiago de Compostela, Spain
[b] REBUSC. Estación de Bioloxía Mariña da Graña, Universidade de Santiago de Compostela, A Graña, Ferrol, A Coruña, Spain
[c] Departamento. Biología Vegetal y Ciencia del Suelo, Universidade de Vigo, 32004 Ourense, Spain
[d] Stanford Synchrotron Radiation Lightsource, SLAC National Accelerator Laboratory, Menlo Park, CA 94025, USA
[e] Department of Environmental Sciences, University of California, Riverside, CA 92521, USA
[f] Luiz de Queiroz College of Agriculture, University of Sao Paulo (ESALQ-USP), Av. Padua Dias 11, CEP 13418-900, Piracicaba, Sao Paulo, Brazil
[g] Universidad Autónoma de Baja California, Instituto de Investigaciones Oceanológicas, Carretera Transpeninsular Ensenada-Tijuana No. 3917, Fraccionamiento Playitas, C.P. 22860 Ensenada, B.C., Mexico
[h] Department of Geography, University of São Paulo, Av. Prof. Lineu Prestes, 338, Cidade Universitária, 05508-900, São Paulo, SP, Brazil

ARTICLE INFO

Editor: Dr. Adina Paytan

Keywords:
Mn speciation
Methane
Pyritization
Anaerobic oxidation of methane (AOM)

ABSTRACT

Manganese is one of the most abundant elements in marine sediments and plays an essential role in sediment redox processes. However, unlike Fe or S, the Mn cycle has not received the same attention. Mn is a ubiquitous redox-active metal in marine systems; however, its influence on C and S cycling is still poorly understood. In particular, we hypothesize that conditions that favor high H_2S production can lead to high Mn pyritization. In the Ria de Vigo, large methane fields have been identified at different depths within sediments, ranging from the surface to 2 m below the surface. Four sediment cores from different locations (outermost, middle, and innermost) within the Ria de Vigo were analyzed. Samples were subjected to a general characterization and a five-step Mn sequential extraction procedure, and analyses were complemented with X-ray absorption spectroscopy (EXAS). The results showed that the main geochemical forms of Mn undergo intense spatial and depth-related variations in sediments. Two geochemical scenarios were identified: one corresponding to the innermost section and another one to the middle and outermost sections of the ria. The former was characterized by intense Mn pyritization and by the absence of the Mn-carbonate fraction due to the high production of H_2S because of anaerobic oxidation of methane. The formation of Mn—S bonds was only identified by EXAS. Conversely, in the middle and outermost part of the ria, with or without the presence of methanogenesis in deep sediment layers, the Mn-carbonate fraction was dominant even at depth, along with the presence of methane, high concentrations of H_2S and, therefore, high degrees of Fe pyritization. These results suggest that, once Mn-carbonate is formed under suboxic conditions (with low or no presence of H_2S) at or near the surface, it remains stable after burial, even under conditions of high H_2S concentration.

1. Introduction

Galician rias are marine systems that are almost exclusively found along the NW coast of the Iberian Peninsula. They support a rich marine biota and are considered one of the most productive marine ecosystems in the world (Álvarez-Salgado et al., 2000; Figueiras et al., 2002). Their high biological production and diversity are the result of upwelling events, which generally occur in spring (March–April) and in fall (September–October) (Souto et al., 2003). These oceanographic events increase primary production through the input of cold, nutrient-rich deep water into the waters of the rias (Prego, 1993; Tenore et al., 1995). In these productive ecosystems, high amounts of organic matter are deposited onto the seabed (e.g. Ramírez-Pérez et al., 2017; Vilas, 2002), promoting the development of anoxic zones and the eventual generation of methane. The existence of methane gas fields (~24.8 km^2; García-Gil et al., 2015) has been identified along modern sediments of

* Corresponding author at: CRETUS. Dpto. Edafoloxía e Química Agrícola, Universidade de Santiago de Compostela, 15782 Santiago de Compostela, Spain.
E-mail address: xl.otero@usc.es (X.L. Otero).

https://doi.org/10.1016/j.margeo.2024.107250
Received 9 March 2023; Received in revised form 2 February 2024; Accepted 24 February 2024
Available online 1 March 2024

the Ria de Vigo (García-García et al., 2005; Martínez-Carreño and García-Gil, 2013).

Due to the high content of organic matter in the sediments of the Ria de Vigo, strongly reducing conditions prevail in these sediments, even in the surface layer (Eh < −150 mV; Ramírez-Pérez et al., 2015, 2020). In marine environments, due to the high sulfate concentrations in seawater, oxidation of organic matter is mainly coupled to bacterial sulfate reduction (Kasten and Jørgensen, 2000). However, other elements such as Fe(III) and Mn(IV) are also involved in the process of organic matter mineralization and can also participate in anaerobic oxidation of methane (AOM) (Beal et al., 2009). Most studies have focused on the influence of Fe(III) on AOM (Holmkvist et al., 2011a, 2011b; Segarra et al., 2013). In general, the process of anaerobic oxidation of methane (AOM) is important, as it is linked to the carbon cycle (Ettwig et al., 2016) and contributes to maintaining methane gas stability by controlling its flux into the atmosphere (Sivan et al., 2011; Ettwig et al., 2016). Methane is the second most important greenhouse gas after carbon dioxide (CO_2), with a warming potential 28–34 times that of CO_2 (Myhre et al., 2013). In the case of Mn(IV)-bearing minerals, widely distributed in the biosphere, Mn-associated AOM could represent a significant global methane sink (e.g., Beal et al., 2009; Egger et al., 2015; Leu et al., 2020), especially considering that ~19 teragrams (Tg) of Mn are annually delivered by rivers to continental margins (Poulton and Raiswell, 2000) and that Mn can undergo oxidation and reduction 100 to 300 times before burial (Canfield, 1989). Finally, it is crucial to note that the Mn-dependent AOM process may have been more prominent in Proterozoic oceans than at present, given the lower concentrations of dissolved sulfate present during that period (Beal et al., 2009). Thus, it is important to collect field evidence for Mn-dependent AOM in marine sediments to adequately assess its significance in methane dynamics.

In the Galician rias, a good number of studies on sediment origin, composition, quality (Rubio et al., 2000, Vilas et al., 1995, Otero et al., 2005, 2006, Guevara, 2020), and presence of methane gas (García-Gil et al., 2011, Ramírez-Pérez et al., 2015, Martínez-Carreño and García-Gil, 2017) have been carried out. Recently, Fe has also been the subject of attention, with several studies establishing the geochemical forms of Fe, Mn, and trace metals in sediments of the Galician rias (Otero et al., 2005; Ramírez-Pérez et al., 2017, 2020); however, information about Mn geochemistry in methane-rich environments is still scarce. In this sense, the main objective of this study was to evaluate the geochemical behavior of Mn in different geochemical environments (presence/absence of methane) in sediments of the Ria de Vigo (NW Spain). Previous studies have divided the Ria de Vigo into three main sections (innermost, middle, and outermost) depending on their hydrological conditions, with the presence of methane gas fields being detected (Ramírez-Pérez et al., 2015; Martínez-Carreño and García-Gil, 2017). According to the presence of methane in sediments of the Ria de Vigo, three geochemical environments can be defined: 1) absence of methane, 2) presence of methane at depth (>80 cm deep), and 3) presence of methane on the surface, with methane being released to the water layer (Ferrín et al., 2003; Iglesias and Garcia-San Gil, 2007; Martínez-Carreño and García-Gil, 2017). As these geochemical conditions are not too frequent in the seabed, sediments of the Ria de Vigo are of particular interest for the study of diagenetic processes on metals. Mn is one of the main redox-sensitive metals that act as electron acceptors in the respiratory degradation of organic matter by heterotrophic bacteria (Thamdrup et al., 1994). Manganese oxide enrichment is common in the surface layer of normal marine sediments (i.e. those that are oxic on the surface and become anoxic in depth; Berner, 1984), as Mn^{2+} diffuses into the oxic zone (Thamdrup et al., 1994; Otero et al., 2009) and can subsequently be reduced again upon downward transport (Aller, 1980; Sundby Bjørn and Silverberg, 1985). Mn enrichment has also been observed on the surface of sediments overlain by anoxic bottom waters (Calvert and Pedersen, 1993; Russell and Morford, 2001). Typically, these enrichments consist of authigenic Mn-carbonate phases, often associated with considerable amounts of calcium (e.g. Ca rhodochrosite and kutnahorite; Suess, 1979; Middelburg et al., 1987). Finally, there are indications that the formation of Mn-sulfides in sediments is also possible, especially when Fe availability is low (Böttcher and Huckriede, 1997; Lepland and Stevens, 1998); nevertheless, Mn pyritization levels observed in marine sediments are generally low (Huerta-Diaz and Morse, 1992; Morse and Luther III, 1999). In order to understand the behavior of Mn in sediments of the Ria de Vigo, we have studied four cores collected in different geochemical environments. For this purpose, Mn was sequentially extracted into different fractions: exchangeable, Mn-carbonate, associated with amorphous iron oxides, associated with crystalline iron oxides, and Mn-pyrite. The results were complemented with X-ray absorption spectroscopic measurements to obtain additional insights into the average oxidation state, coordination environment and dominant mineral host phase of Mn.

2. Material and methods

2.1. Environmental setting

The Ria de Vigo is located on the southwest Atlantic coast of Galicia (NW Spain) (Fig. 1). This ria is a large submerged and incised valley with a total area of 176 km^2. Water depth ranges from <7 m in San Simon Bay to 50 m in the southern mouth of the ria, with average salinity ranging between <32 at the innermost section (San Simon Bay) and 36 in the outermost section of the ria (Torres López et al., 2001). San Simon Bay is a small, NS-oriented shallow basin located in the innermost part of the ria. It is 10 km long and 4 km wide, with a total area of 19.5 km^2. This bay is connected to the ria by a narrow channel, the Rande Strait, which is 600 m wide and 1.5 km long (Martínez-Carreño and García-Gil, 2013; García-Gil et al., 2011). Previous works have shown that in San Simon Bay, where one of our cores was obtained, methane bubbles come out towards the water layer during the summer (García-Gil et al., 2011). However, in the core studied in this work, the presence of methane was observed at a sediment depth of 80 cm (Ramírez-Pérez et al., 2015).

Upwelling processes provide cold, nutrient-rich waters, leading to high productivity, thus providing an ideal location for intense mussel farming (with around 483 mussel rafts: https://www.mexillondegalicia.org/cultivo/la-rias/), which increases the flow of organic matter to the seabed, leading to average total organic carbon (TOC) values in sediments ranging from 7% to 10% (Vilas et al., 1995; Otero et al., 2005). The TOC/TN ratio ranges from 8 to 20, suggesting a mixed (marine and continental) origin of organic matter (García-Gil et al., 2011). Sediments are fine-grained, with pH values close to neutral or slightly alkaline and with strongly reduced Eh values (generally Eh < −50 to −150 mV); these conditions indicate anaerobic degradation of organic matter, as well as biogenic methane production (García-Gil et al., 2011; Ramírez-Pérez et al., 2015). Shallow gas accumulations have been observed in the Holocene sedimentary record (Martínez-Carreño and García-Gil, 2013), with a delimited sulfate-methane transition zone (SMTZ) between 80 and 100 cm of sediment depth in the innermost section, and between 200 and 220 cm depth in the outermost section of the Ria de Vigo (see Ramírez-Pérez et al., 2015, for further details). The uppermost sediments of the Ria de Vigo showed sulfate concentrations close to those of the water column (28 mM), which quickly decreased in the sediment column in the presence of methane (see Ramírez-Pérez et al., 2015; Table 1). Sediments show high degrees of pyritization (DOP >39%), with marked increases in areas where methane is present (DOP>65%, Ramírez-Pérez et al., 2015, 2017; see Table 1). In the innermost section of the ria, where methane is present at shallower sediment depths, iron pyrite is present in their uppermost portions (Ramírez-Pérez et al., 2020), which highlights the effect of methane on the marine Fe and S cycles. In addition, AVS concentration is very low for all sites, generally below 0.50 μmol g^{-1}, with the highest values corresponding to the upper portions of the innermost zone (0.73 ± 0.43 μmol g^{-1}; Ramírez-Pérez et al., 2020; Table 1).

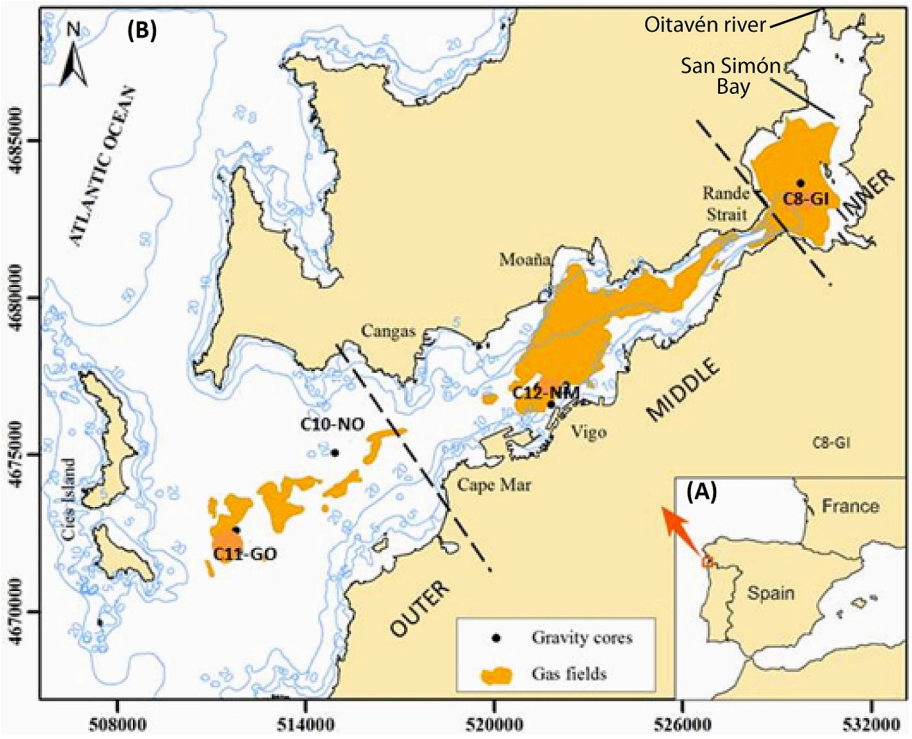

Fig. 1. (A) Location of the Ria de Vigo. (B) Location of cores in the Ria de Vigo in relation to methane fields. Core C11 was not considered for this study.

Table 1
General characteristics of the studied gravity cores (Data from Ramirez-Pérez et al., 2015, 2017).

	Cores			
	C10-NO	C11-GO	C12-NM	C8-GI
pH	7.1–7.7	7.2–8.0	7.1–8.0	6.9–7.9
Eh (mV)	−112- +53	−53- -178	−78- -187	−168- -192
Methane (mM)	–	0.00–4.40	–	0.00–0.89
Pore water sulfate (mM)	9.46–24.79	0.03–33.67	8.12–28.17	0.05–28.89
Pore water sulfide (mM)	0.00–2.33	0.00–7.69	0.01–8.77	0.34–18.51
Depth of SMTZ* (cm)	–	200–220	–	80–100
Exchangeable Fe (μmol g^{-1})	0. 00–0.17	0.00–0.11	–	–
Carbonate Fe (μmol g^{-1})	0.48–8,66	0.00–9.54	2.22–11.28	0–5.72
Amorphous Fe oxyhydr. (μmol g^{-1})	45.85–121.50	38.68–99,22	81.45–114.86	37.43–80.25
Crystalline Fe oxyhydr. (μmol g^{-1})	14.38–313.74	7.11–140.42	14.63–195.33	5.16–45.43
Pyrite Fe (μmol g^{-1})	34.77–225.00	19.44–253.17	14.00–193.40	80.32–176.46
DOP (%)	11.72–72.67	7.52–70.63	4.95–61.57	47.28–75.19

* SMTZ: sulfate-methane transition zone depth.

2.2. Sampling sites

Four gravity cores were collected from the Ria de Vigo (Fig. 1) in November 2012 aboard the R/V *Mytillus;* these were the same cores studied by Ramírez-Pérez et al. (2015), Ramírez-Pérez et al., 2020). Sampling sites in the Ria de Vigo were selected based on geographical location (I: innermost section; M: middle section; O: outermost section) and on the distribution of mapped methane gas fields (G: with gas; N: without gas) previously identified by Iglesias and Garcia-San Gil (2007) and García-Gil et al. (2011). Cores C8-GI and C11-GO were located within gas fields (Fig. 1; Supplementary information), with the former collected in San Simon Bay and in the innermost part of the Ria where presence of methane gas was detected at a depth of ~90 cm. However, some authors have reported methane bubbling at the sediment surface of this site and have quantified the emission of methane to the atmosphere at 7.0 to 34.2 t y^{-1} (Ferrín et al., 2003; Iglesias and Garcia-San Gil, 2007; García-Gil et al., 2011). The second gravity core, C11-GO, collected in the outermost section of the ria, which is under dominant oceanic influence, showed presence of methane from a sediment depth of 220 cm (Ramírez-Pérez et al., 2015). The remaining cores were collected outside of gas fields in the middle and outermost sections (C12-NM and C10-NO, respectively), both under dominant oceanic influence. In order to minimize oxidation of the collected material, cores were sliced into 2.5-com sections on board in the ship's laboratory, then placed in plastic bags and immediately frozen at −18°C until chemical analysis.

2.3. Mn geochemical forms extraction

The extraction of Mn was carried out on bulk wet sediment samples by combining the sequential extraction procedures by Tessier et al. (1979), with small modifications to allow for the separation of easily reducible Mn forms into those associated with crystalline Fe oxy-hydroxides, according to the method by Fortin et al. (1993), and of the pyrite fraction, according to the method by Huerta-Diaz and Morse (1990), Huerta-Diaz and Morse, 1992). This combination of methods, similar to those used by other authors (e. g. Yu et al., 2015; Otero et al.,

2009), allows for the differentiation of five different fractions, according to the following classification:

- *Fraction F1: exchangeable Mn.* 1 g of wet sediment was extracted with 30 mL of 1 M $MgCl_2$ solution at pH 7 (adjusted with concentrated acetic acid) at 4°C with continuous stirring for 30 min, centrifuged at 10,000 rpm at 4°C for 20 min, and filtered through Albet filter paper. The extract was stored at 3°C until analysis. The residue was washed twice with 20 mL of deoxygenated Milli-Q water (18 Ω) before starting the next extraction step. The same centrifugation, filtration, and washing procedures were repeated at the end of each of the following extraction steps.
- *Fraction F2: Mn associated with carbonates.* Extracted with 30 mL of 1 M NaOAc at pH 5; samples were shaken for 5 h at room temperature.
- *Fraction F3: Mn associated with amorphous iron oxides (easily reducible Mn (*e.g. *Ferrihydrite or Lepidocrocite)*. Extracted with 30 mL of 0.04 M hydroxylamine hydrochloride? + acetic acid (25% *v*/v) solution, shaking the samples for 6 h at 96°C.
- *Fraction F4: Mn associated with crystalline iron oxides (*e.g. *goethite or hematite)*. Extracted using 20 mL of 0.25 M sodium citrate +0.11 M sodium bicarbonate with 3 g sodium dithionite solution, shaking for 30 min at 75°C.
- *Fraction F5: Mn associated with pyrite*. Extracted using 10 mL of concentrated HNO_3; samples were shaken for 2 h at room temperature. Before extracting this fraction, samples were pretreated with 30 mL of 10 M HF, constantly shaking at room temperature for 16 h to eliminate silicate-associated Mn, followed by a 2 h digestion with 15 mL concentrated H_2SO_4 to eliminate the Mn bound to organic matter (Huerta-Diaz and Morse, 1990; Huerta-Diaz and Morse, 1992).

The degree of Mn pyritization (DTMP-Mn), as proposed by Huerta-Diaz and Morse (1990), provides an estimate of the content of a particular metal incorporated into the pyritic phase. DTMP-Mn was calculated according to eq. 1, which defines reactive Mn as the sum of fractions F1 to F5 ($\sum F1_{Mn} \rightarrow F5_{Mn}$).

$$\mathrm{DTMP-Mn}\ (\%) = [(\mathrm{Mn-pyrite})/(\mathrm{Reactive\ Mn})]\ \mathrm{x}\ 100 \quad (1)$$

Manganese concentrations were determined by flame atomic-absorption spectrophotometry (Perkin-Elmer model PinAAcle 500). An aliquot of each sediment sample was dried at 110°C to calculate the percent humidity, expressing the results as dry weight.

2.4. X-ray absorption spectroscopy

X-ray absorption spectra were measured at the Mn K-edge Stanford Synchrotron Radiation Lightsource at beamline 11–2, a 26-pole 2 T wiggler end station, under standard ring conditions of 3 GeV and 500 mA. Energy selection was provided by a Si (220) double crystal monochromator with a crystal orientation of $\phi = 90$, and higher-order harmonics were excluded using a Rh-coated mirror. All spectra were collected in fluorescence mode using a Canberra 100-pixel monolithic solid state Ge detector array. All samples were analyzed at room temperature in a He-purged vessel to exclude the presence of oxygen, using an in-line Mn foil as a reference. The inflection point of the rising edge was calibrated to 6539 eV, and no photodamage was observed across multiple scans of the same sample. Data presented here represent the average of eight scans per sample. Spectra were collected on cores C8-GI (20–22.5 cm and 90–92 cm depth; X-ray absorption spectra codes 88C8 and 160C8, respectively), C10-NO (50–52.5 cm depth; 88core10), and C11-GO (50–52.5 cm depth, 17core11).

All channels were inspected for possible contamination by elastic scatter prior to averaging using Larch (version 9.61 Windows) (Newville, 2013). Calibration, normalization, and merging of replicate scans were performed using the Demeter package (version 9.26) (Ravel and Newville, 2005) with Larch running as a backend (Newville, 2013) on Windows 10. The average Mn oxidation number (AMON) for each sample was obtained through linear combination fitting analysis of the Mn X-ray absorption near-edge structure (XANES) spectra and was performed in Athena (Ravel and Newville, 2005) using the Combo method by Manceau et al. (2012). In all cases, reference spectra from 12 pure-valent Mn species were used to perform unconstrained linear fits. Any reference yielding a negative loading was progressively removed on a per-sample basis and re-added to the reference list before fitting the next sample. The MnII, MnIII, and MnIV fractions and AMON were calculated from the fits according to Manceau et al. (2012). A paired-sample *t*-test was used to assess the difference between the means of the AMON data corresponding to soil samples. For the assessment of the relative fraction of Mn distributed between adsorbed MnII and Mn oxide phases, linear combination fitting of EXAFS was used. For this technique, three MnII standards, 6 MnIII,IV oxides, and 2 Mn oxides containing MnII were used to fit the spectra. EXAFS references were a mixture of spectra collected in-house and those obtained by Santelli et al. (2011). The fractional weights for all oxide phases were combined and compared with the combined weight of the MnII standards prior to comparison of means through a paired-sample *t*-test. Fits were conducted between K = 3 and K = 11. XANES and EXAFS data from the standards used in all linear combination fitting, as well as XANES linear combination fittings and data, are available in the SI.

2.5. Statistical analysis

In this work, the surface layer (≤30 cm depth) was defined as the portion of the sediment column subjected to physical perturbations produced by marine and tidal currents as well as biophysical reworking produced by biota (Burdige, 1993). A one-way ANOVA was used to test equality of means when data were shown to follow a normal distribution and homogeneity of variance, while the Mann-Whitney *U* test was used as a nonparametric test to identify differences in medians of selected variables between surface (<30 cm depth) and deep sediments. The relationships between the different variables were tested using Spearman's correlation coefficients. Differences were considered significant at $p < 0.05$. All statistical analyses were carried out using the software SigmaPlot (version 11.0).

3. Results

3.1. Reactive Mn in sediments of the Ria de Vigo

Reactive Mn ($\sum F1_{Mn} \rightarrow F5_{Mn}$) ranged between 386 and 2248 nmol g^{-1} (21.2–124 mg kg^{-1}), with an average value of (10.3 ± 3.7)x10^2 nmol g^{-1} (57 ± 20 mg kg^{-1}) for the whole set of samples (Table 2). The lowest content was found in the innermost section of the ria (C8-GI; mean value: 618 ± 99 nmol g^{-1}), with increasing values towards its outermost section (middle section: 694 nmol g^{-1}, outermost section: 1929 nmol g^{-1}; Fig. 2). In all cores, the concentrations of reactive Mn and of the geochemical fractions mentioned below showed abnormally high values at certain depths, which were associated with sediment layers with finer textures (see Ramírez-Pérez et al., 2015, 2017).

3.2. Geochemical forms of Mn

Distribution of manganese geochemical fractions along the Ria de Vigo is shown in Fig. 2 and Table 2. In general, fraction F3 (Mn associated with amorphous iron oxides) was the dominant fraction in surface sediments (38–68%; Table 2), followed by F2 (carbonate fraction: 0–44%); however, below 30 cm depth, the dominant fraction was Mn-pyrite (49–71%). Fraction F1 was below the limit of detection (LD ~ 5 nmol g^{-1} d.w.; Otero et al., 2003) in most samples (Fig. 2). However, it is worth noting that the geochemical behavior of Mn showed a wide

Table 2
Average concentrations of Mn associated to different geochemical fractions as well as degree of Mn pyritization (DTMP-Mn) and percentage of carbonate fraction in sediments of the ría de Vigo relative to depth and presence/absence of methane. For the same column different letters indicate significant differences ($p < 0.05$).

Sample	Mn Reactive	Mn carbonate	Mn oxyhydroxides	Mn Pyrite	Mn DTMP	Carbonate fraction
	(nmol g^{-1})				(%)	
Surficial sediments without methane	$(10.9 \pm 2.5)x10^2$	$(3.3 \pm 1.1)x10^{2\ (b)}$	$215 \pm 47^{(c)}$	$13 \pm 34^{(a)}$	$1.3 \pm 3.3^{(a)}$	$30 \pm 4^{(b)}$
Deep sediments without methane	$(12.5 \pm 3.7)x10^2$	$414 \pm 30^{(bc)}$	$94 \pm 221^{(b)}$	$(2.5 \pm 2.1)x10^{2(b)}$	$18 \pm 17^{(b)}$	$36 \pm 12^{(c)}$
Surficial sediments with methane at depth	$(9.9 \pm 3.2)x10^2$	$514 \pm 29^{(c)}$	$228 \pm 18^{(b)}$	$0 \pm 0^{(a)}$	$0 \pm 0^{(a)}$	$40 \pm 2^{(c)}$
Deep sediments with methane	$(8.5 \pm 3.6)x10^2$	$(4.5 \pm 2.2)x10^{2\ (bc)}$	$16 \pm 50^{(a)}$	$(3.1 \pm 2.1)x10^{2\ (bc)}$	$27 \pm 15^{(b)}$	$38 \pm 12^{(c)}$
Surficial sediments with methane (inner zone, San Simon bay)	$(7.1 \pm 1.6)x10^2$	$0 \pm 0^{(a)}$	$0 \pm 0^{(a)}$	$(3.3 \pm 1.8)x10^{2\ (c)}$	$44 \pm 12^{(c)}$	$0 \pm 0^{(a)}$
Deep sediments with methane (inner zone, San Simon Bay)	579 ± 98	$0 \pm 0^{(a)}$	$0 \pm 0^{(a)}$	$289 \pm 88^{(c)}$	$49 \pm 8^{(c)}$	$0 \pm 0^{(a)}$

spatial variability. Fraction F3, corresponding to easily reducible Mn and Fe forms (Tessier et al., 1979), showed high values in all cores and for all depths (fraction F3: 562–243 nmol g^{-1}; Fig. 2), even in those cores where methane was present. On the other hand, fraction F4, which corresponds mainly to Mn associated with crystalline Fe oxyhydroxides, showed moderate surface concentrations (fraction F3 0–30 cm: 134–274 nmol g^{-1}), except for core C8-GI, where the concentration of Mn associated with fraction F4 was below the limit of detection at the surface (LD ~ 5 nmol g^{-1}; Otero et al., 2003), as well as throughout the whole core (Fig. 2). Below a depth of 100–125 cm, Mn associated with fraction F4 showed values < LD for almost all samples from the four cores analyzed in this study.

The geochemical behavior of Mn showed both depth-related and spatial variability, with samples from the sediments of the innermost section of the Ria de Vigo (San Simon Bay, core C8-GI) showing the greatest differences relative to the cores collected from the remaining sites (Table 2). In this core, only the concentrations of Mn associated with amorphous Fe oxides (F3) and Mn-pyrite (F5) were detected (Fig. 2 and Table 2). Manganese associated with the exchangeable (F1), carbonate (F2), and crystalline oxyhydroxide (F4) fractions were below their corresponding detection limits for the whole core. Manganese contents associated with amorphous Fe oxides were more homogeneous throughout this core and slightly lower than those observed in the middle and outermost sections of the ria, with a mean value of 316 ± 53 nmol g^{-1}, a result that could be related to a methodological issue (see Discussion section below). The value of $(3.0 \pm 1.2)x10^2$ nmol g^{-1} obtained for the Mn-pyrite fraction (301 ± 119 nmol g^{-1}) corresponded to the highest content in the uppermost sediment layers, with a maximum content of 669 nmol g^{-1} at a depth of 20 cm. Below this depth, contents ranged from 143 to 433 nmol g^{-1}.

In the middle section of the Ria de Vigo (core C12-NM), Mn content in fraction F1 was <LD, while its concentration in fraction F2 showed high values (297 ± 89 nmol g^{-1}). Mn-carbonate (fraction F2) content increased rapidly from the core surface down to 100 cm depth, reaching a maximum concentration of 523 nmol g^{-1}. Below this depth, Mn-carbonate content decreased with depth down to a value of 251 nmol g^{-1}. Manganese concentrations associated with fractions F3 and F4 were relatively constant along the upper 100 cm (445 ± 50 nmol g^{-1}) and 50 cm (179 ± 25 nmol g^{-1}), respectively, and were < LD below 100 cm depth. Mn-pyrite rapidly increased in concentration below 20 cm depth, reaching a maximum value of 487 nmol g^{-1} at a depth of 100 cm.

In the outermost section of the ria (C11-GO and C10-NM), exchangeable Mn (F1) was the fraction that showed the lowest Mn content. In core C11-GO, this fraction was only detected at 50 cm depth (64 nmol g^{-1}), while in core C10-NO, it was detected between 100 and 225 cm depth (50–97 nmol g^{-1}). The dominant form of Mn in this section was associated with the carbonate fraction, with concentrations varying between 196 and 814 nmol g^{-1} and 186 and 807 nmol g^{-1} in cores C11-GO and C10-NM, respectively. Mn associated with F3 ranged from 253 to 656 nmol g^{-1}, with the lowest values corresponding to the core with presence of methane (C11-GO). This fraction experienced a slight decrease with depth in both cores (Fig. 2). Mn associated with crystalline Fe oxyhydroxides was only detected in the uppermost portion of both cores, although it is worth highlighting that in the core without methane (C10-NM), Mn—F4 was detected down to a depth of 125 cm (234 ± 16 nmol g^{-1}), while in the core with presence of methane (C11-GO), it was detected only down to 50 cm depth (221 ± 24 nmol g^{-1}). Interestingly, Mn-pyrite (F5) behaved inversely to Mn—F4 with increasing depth: in core C11-GO [$(3.4 \pm 1.8)x10^2$ nmol g^{-1}], it was detected only below 50 cm depth, while in core C10-NM [$(2.3 \pm 2.2)x10^2$ nmol g^{-1}] it was detected below 100 cm depth. In both cores, an increase in Mn-pyrite content with depth was observed, reaching a maximum value of 754 nmol g^{-1} in core C11-GO.

3.3. Degree of manganese pyritization (DTMP-Mn)

DTMP-Mn, which also showed a high spatial and depth-related variability in sediments of the Ria de Vigo (Fig. 3 and Table 2), increased from the outermost section (mean DTMP-Mn value: 21 ± 17%) towards the innermost section of the ria (mean DTMP-Mn value: 48 ± 9%).

In the innermost section (C8-GI), high DTMP-Mn values were observed already in the uppermost layer (DTMP-Mn: 32%), sharply increasing from the surface down to 30 cm depth (DTMP-Mn: 67%), while below this depth, values ranged between 37% and 60%. In the middle section (C12-NM), Mn pyritization started below a depth of 20 cm, with an average value of around 6 ± 5% between 20 and 50 cm depth. From the surface down to a depth of 100 cm, DTMP-Mn values increased from 2% to 32%, with values within the 21%–38% range between 100 cm depth and the bottom portion of the sediment core. Differences in DTMP-Mn were observed between cores C10-NO (methane absent: 20%) and C11-GO (methane present: 30%), retrieved in the outermost section of the ria (Fig. 3). Finally, it is worth noting that DTMP-Mn showed a highly significant negative correlation with Mn-carbonate concentration (Fig. 4).

3.4. XANES and EXAFS characterization

The spectra obtained from each of the four core sections were comparable in terms of the shape and intensity of their pre- and post-edge features, an indication of similar host-mineral phases. However, post-edge features were poorly modelled by the Combo method for the estimation of Mn AOS, indicating that the form of Mn in our samples was not detected by any of the standards employed in the analysis. However, it was able to accurately model the edge position, which is frequently used in the determination of oxidation state among samples of metals with similar spins and ligand environments. In all cases, AOS was measured at +2.3, indicative of a mixed valence Mn(II)-Mn(III) system (Table 3), and

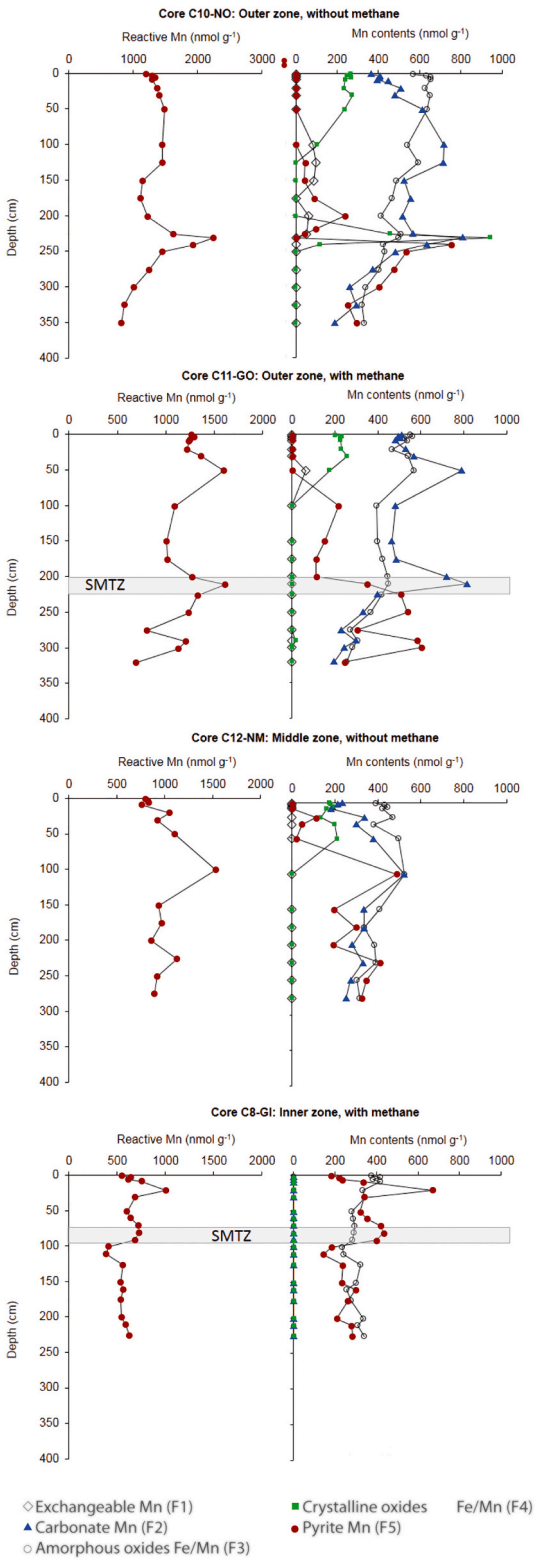

Fig. 2. Manganese concentrations in different sedimentary geochemical fractions: exchangeable (F1), associated with carbonates (F2), associated with amorphous iron oxides (F3), associated with crystalline iron oxides (F4), associated with pyrite (F5), and reactive fraction (∑F1 → F5). SMTZ: sulfate-methane transition zone.

all standards except for Hureaulite (a hydrated Mn(II) phosphate hydroxide) and Mn_2O_3 were rejected from the fit. Modeling of the pre-edge features yielded fit centroids and areas consistent with mixed-valence Mn(II)-Mn(III) amphiboles, such as richterite, with reported AOS values of 2.1–2.5, consistent with the AOS value of +2.3 reported here (Fig. 5) (Chalmin et al., 2009). For all samples, the fit centroid ranged from 6540.6 eV to 6540.9 eV, with the centers of the three pseudo-Voigt functions used in the model at approximately 6539.9 eV, 6541.1 eV and 6542.6 eV, respectively (Appendix Table S1).

The bonding environment of Mn in silicate minerals is complex, with four distinct sites for Mn substitution present in richterite alone (Oberti et al., 2000, Chalmin et al., 2009; Lenz et al., 2014a, Lenz et al., 2014b). This complexity, along with the addition of non-silicate Mn phases (e.g. Mn-pyrite) and truncation of the data due to the Fe k-edge, precluded conclusive EXAFS analysis of the exact Mn coordination environment. This phase heterogeneity, coupled with the measurements being taken at room temperature, resulted in large values of σ^2, leading to additional dampening of the signal. However, first shell fits were performed to test whether the Mn coordination environment was dominated by O or S (Appendix Table S2 and Fig. 6). In 88core10 and 17core11, the Mn—S contribution was rejected and the data were best fit using a split first shell, with approximately one short Mn—O bond and five longer Mn—O bonds. This allowed further fitting Mn—Si and Mn-Mn/Fe scattering contributions to the data, yielding coordination numbers and distances indicative of Mn-substituted richterite (Della Ventura et al., 1993). When applied to 175core8 and 160core8, the two oxygen-shell models either yielded non-physical σ^2 values or overfit the O contribution and underfit a portion of the first shell at higher radial distance, indicating that a heavier coordinator (S) was needed. These samples were then fit by assuming that Mn was coordinated by six atoms in both the oxide and sulfide phases and then fitting the first shell to allow the proportions of these contributions to float. Both sections of core8 showed evidence of >12% Mn—S, as well as Mn—Si and Mn-Mn/Fe scattering, indicative of the predominant Mn-silicate host phase.

4. Discussion

Mn is one of the most abundant trace metals in the lithosphere, with mean values around 1000 mg kg^{-1} (Pais and Jones, 1997). However, sediments of the Ria de Vigo clearly have lower concentrations, ranging from $(1.7 \pm 2.2)x10^2$ mg kg^{-1} in sandy sediments to 224 ± 24 mg kg^{-1} in fine-textured sediments (Rubio et al., 2000; Segarra et al., 2008).

The Mn XANES support the conclusion that the predominant host mineral phase for Mn are silicate minerals (Tables 3 and Appendix Table S1). Prior work by Lenz et al. (2014a), Lenz et al., 2014b) had identified a Mn host phase with similar spectral features in sediments taken from the Gotland basin in the Baltic Sea (Lenz et al., 2014a, Lenz et al., 2014b). In this study, the Mn phase was identified as richterite, a K-amphibole found in peridotite into which Mn(II) readily substitutes for Mg(II) (Welch, 2021; Holtstam et al., 2019). These authors found that the presence of Mn could be attributed to detrital phyllosilicates that accumulated in the sediments at a constant rate, although their source was not defined (Lenz et al., 2014a, Lenz et al., 2014b). The XANES of Mn-substituted richterite was later described by Chalmin et al. (2009), showing features similar to the Mn XANES obtained for our samples, notably a prominent shoulder on the rising edge at 6548 eV and two peaks in the white line region at 6552 eV and 6557 eV (Fig. 6).

K-richterite is a dominant hydrous phase of the upper mantle (Welch, 2021), and its presence in sediments of the ria is likely due to both fluvial contributions from deposits in the surrounding landscape and in-situ weathering. This contention is supported by earlier work by Belzunce-Segarra et al. (2002), who reported that clay inputs into the Ria de Vigo were dominated by terrestrial inputs via fluvial deposition. Segarra et al. (2008) used an extraction method similar to the one described here and found that Mn in sediments of the Ria de Vigo were largely associated with the residual fraction, indicating that they had a detrital, lithogenic

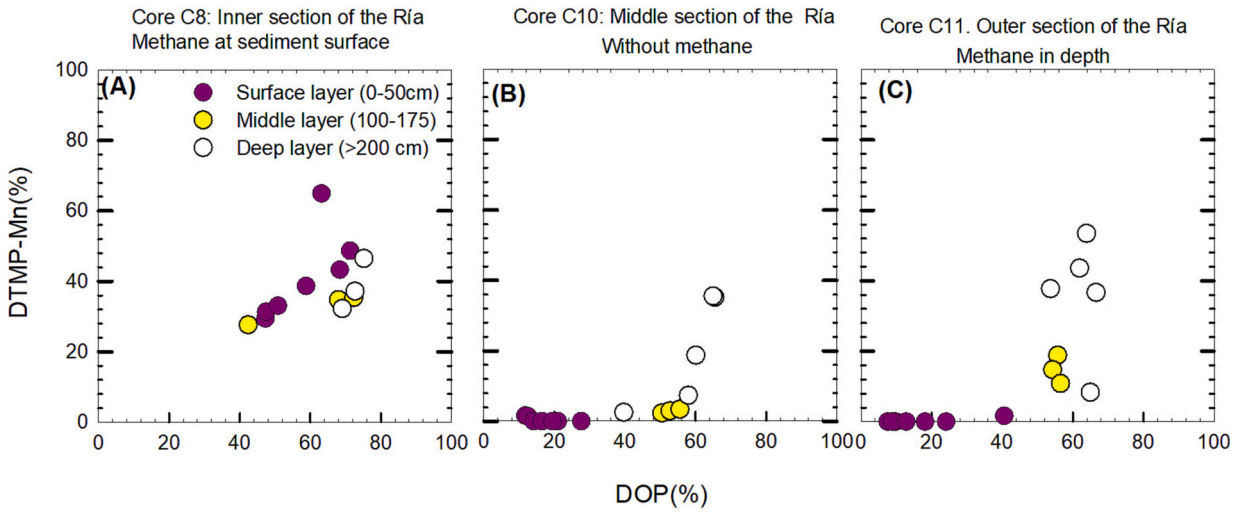

Fig. 3. Degree of Mn pyritization (DTMP-Mn) vs. degree of Fe pyritization (DOP).

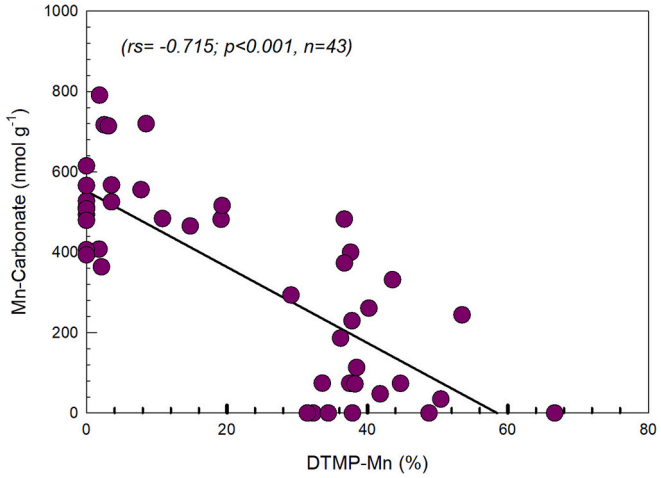

Fig. 4. Degree of Mn pyritization (DTMP-Mn) vs. Mn concentration in the carbonate geochemical fraction (Mn-carbonate). The line represents the best fit for the data.

Table 3
Relative abundance and average oxidation state (AOS) of Mn in sediments from the Ria de Vigo.

Sample	Relative abundance (%)		AOS	χ^2_{red}
	Mn(II)	Mn(III)		
175 Core8 (20–22,5 cm depth)	65	35	2.35 ± 0.05	0.0031
160 Core8 (90–92,5 cm depth)	65	35	2.35 ± 0.06	0.0043
88 Core10 (50–52,5 depth)	69	31	2.31 ± 0.07	0.0058
17 Core11 (50–52,5 cm depth)	66	34	2.34 ± 0.06	0.0053

origin, as would be expected if a host phase such as richterite were their dominant source. This finding is supported by previous works where Mn in surface sediments from the Ria de Vigo, including San Simon Bay, was attributed to detrital terrestrial inputs (Belzunce-Segarra et al., 2002; Howarth et al., 2005). However, the reactive-Mn fraction (i.e. Mn not associated with the silicate fraction) reaches sedimentary areas as coating on other larger particles (e.g. sand or silt), mainly in the form of Mn(IV) oxides and hydroxides (e.g. vernadite or MnO_2; Burdige, 1993), or associated (co-precipitated) with Fe oxides and hydroxides. Mn oxides and hydroxides are characterized by showing low degrees of crystallinity, high specific surface areas, and high adsorption capacity (Glasby, 1984); for these reasons, they are considered easily reducible minerals, being reduced by facultative anaerobic bacteria shortly after the sediment becomes anaerobic (Burdige, 1993).

The final product of the reduction of Mn(IV) is mainly Mn^{2+} and, to a lesser extent, Mn^{3+} (Burdige, 1993), with the former initially becoming part of the interstitial water, either as a free ion or complexed with organic compounds (Elderfield, 1981). Our results showed drastic changes in Mn forms, both spatially and with depth, allowing us to define two geochemical scenarios:

4.1. Scenario 1. Middle and outermost sections of the Ria de Vigo: sediments with or without the presence of methane at depth

From a hydrodynamic point of view, the middle and outermost sections of the ria are characterized by rapid circulation of the water layer and by several deep-water upwelling events every year. The bottom water layer and the upper sediment portion (<5 cm) of the Ria de Vigo have been considered as oxic (Belzunce-Segarra et al., 2008), consistently with the oxic characteristics of the water layer. However, sediments of the ria are anoxic (Eh <35 mV) below 10 cm depth, and their pH is slightly alkaline (pH: 7–8) (Otero et al., 2009; Ramírez-Pérez et al., 2015). Eh-pH diagrams show that under these conditions, Mn remains preferentially in ionic form (Mn^{2+}) (Brookins, 1988). However, some studies have suggested that Mn^{2+} concentration in interstitial water is much lower than predicted by geochemical models, a difference that has been attributed to adsorption processes, precipitation of mixed Mn^{2+}, Mn^{3+}, and Mn^{4+} oxides and hydroxides, or co-precipitation with Fe oxyhydroxides (Alvarez et al., 2005). In sediments of the Ria de Vigo, soluble and exchangeable Mn (Mn^{2+}, fraction F1) constituted a geochemically irrelevant fraction, since its concentrations were below the detection limit for virtually all cores and sediment depths (Fig. 2).

In marine sedimentary environments, Mn^{2+} solubility can be controlled by the carbonate (i.e., precipitating as carbonate; Calvert and Pedersen, 1996; Herndon et al., 2018) or pyritic fractions (i.e., coprecipitating with Fe sulfides; Huerta-Diaz and Morse, 1992). The conditions controlling the solubility of Mn^{2+} in both fractions are still not well established (Herndon et al., 2018). Thus, for example, in sediments from the Guaymas hydrothermal vent (Gulf of California, Mexico), where H_2S emissions occur, intense pyritization was observed for most metals (degree of pyritization of Fe: >95%, Cu: 100%, Zn:100%, Cr: 100%, Ni, 75%, Co: 75%), but not for Mn. In these sediments, Mn was found mainly associated with the carbonate fraction (41 ± 12%) and, to a very low

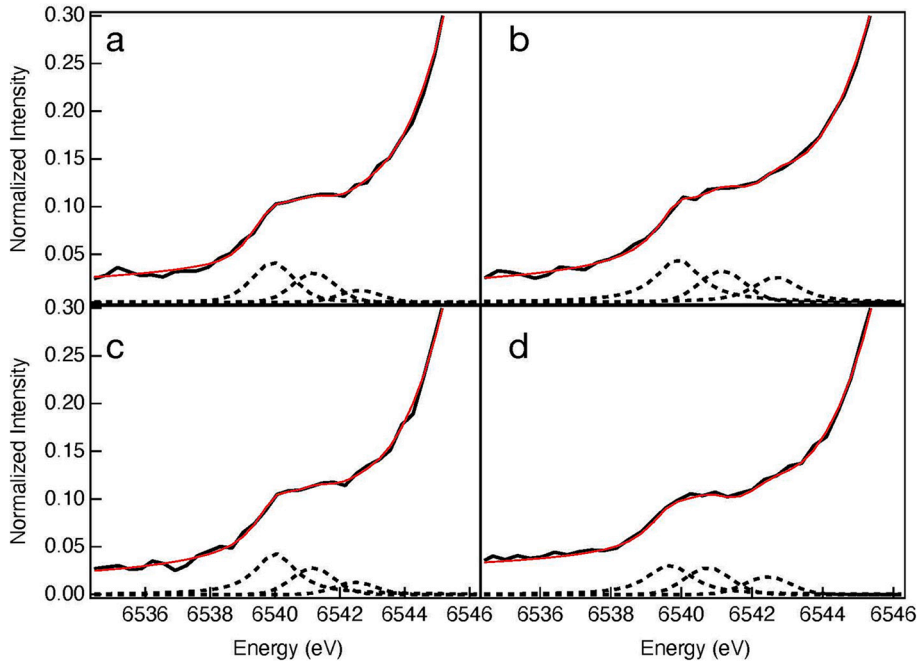

Fig. 5. The Mn XANES pre-edge region where the pre-edge feature has been modelled using pseudo-Voigt peaks. (a) 160Core C8-GI (20–22.5 cm depth); (b) 17Core C11-GO (50–52.5 cm) (c) 160Core C8-GI (90–92.5 cm depth) and (d) 88core C10-NO (50–52.5 cm depth).

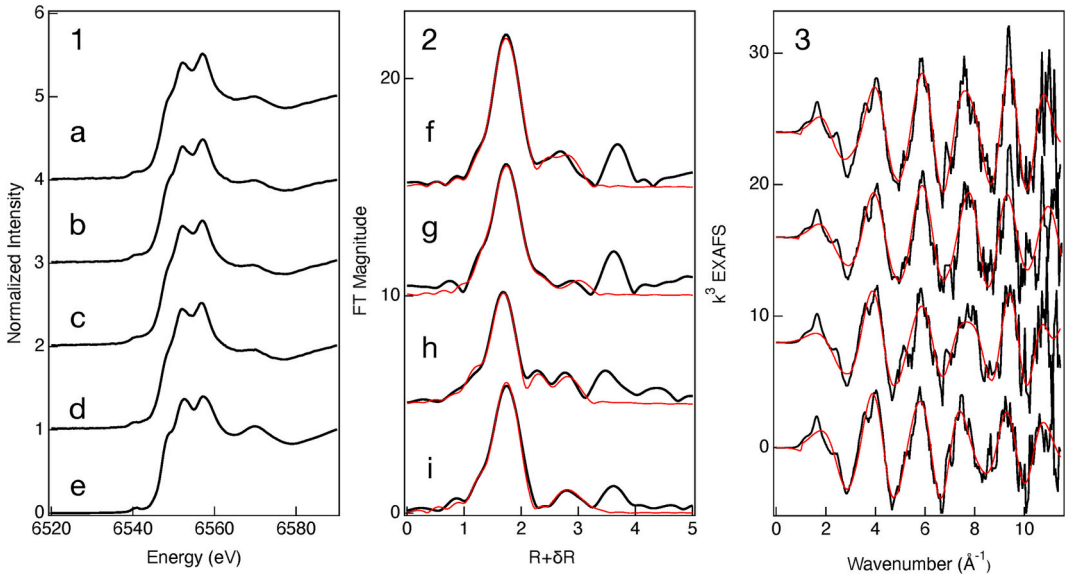

Fig. 6. Mn K-edge x-ray absorption spectra for four cores. Panel 1: Mn XANES. (a) 17core C11-GO (50–52.5 cm depth); (b) 88core C10-NO (50–52.5 cm depth). (c) 175core C8-GI (90–92.5 cm depth); (d) 160core C8-GI (20–22.5 cm depth). Panel 2: Fourier transformed k^3-weighted Mn EXAFS and their corresponding fits. (e) 88core C10-NO (50–52.5 cm depth) with O, Si, and Mn paths. (f) 17core C11-GO (50–52.5 cm depth), O and O fit. (g) 88core C10-NO (50–52.5 cm depth), O and O fit. (h) 175core C8-GI (90–92.5 cm depth), O and S fit. (i) 160core C8-GI (20–22.5 cm depth) fit. Panel 3: k^3 weighted Mn K-edge EXAFS, shown in the same order as in panel 2.

extent, with pyrite (2.7 ± 1.2%) (Otero et al., 2003). Low degrees of Mn pyritization have also been observed in other sedimentary environments such as Atchafalaya Bay (0.62 ± 0.2%; anoxic-non-sulfidic delta sediments) and Orca Basin (0.7 ± 0.7%; euxinic hypersaline sediments) (Huerta-Diaz, 1989). Different DTMP-Mn levels have been found in the Galician rias with, for example, low values in surface sediments of the Ria de Ortigueira (DTMP-Mn 6.4 ± 3%; Guevara, 2020) and high percentages in the Ria de Arousa (DTMP-Mn 47 ± 8%; Otero et al., 2005) and Ria de Ares (23 ± 14%; Macías and Mora, 2001), probably as a result of labile organic matter enrichments in sediments due to mussel farming (Macías, 1999; Otero et al., 2005). Relatively high DTMP-Mn values have also been observed in marsh soils (27 ± 29%; Otero et al., 2003), in Green Canyon (24 ± 13%; natural oil seep with anoxic-sulfidic hemipelagic deep sediments), and in Baffin Bay (DTMP-Mn: 29 ± 12%; anoxic-sulfidic hypersaline coastal lagoon) (Huerta-Diaz and Morse, 1990, Huerta-Diaz and Morse, 1992). In this study, Mn pyritization values ranged from 1.6% to 53.5%, with the highest percentages always found at the deepest portions of cores (Fig. 2). These results indicate that Mn is particularly pyritized to a high extent under conditions of high H_2S production (see also Huerta-Diaz and Morse, 1992; Morse and Luther III,

1999). The free Mn^{2+} ion does not easily form discrete MnS mineral phases (Brookins, 1988) and is generally incorporated into pyrite only at high degrees of iron pyritization (DOP >40–50%) (Huerta-Diaz and Morse, 1992; Morse and Luther III, 1999; Otero and Macías, 2003). Low Fe pyritization entails high environmental concentrations of reactive Fe (i.e., Fe^{2+}), which would compete with Mn^{2+} to precipitate as sulfides. The formation of Fe sulfides is favored over that of Mn sulfides because Fe concentrations generally are two to three orders of magnitude greater than those of Mn; additionally, Mn sulfides (e.g., alabandite, $pK_{sp} = -1.3$; Robie, 1966) are much more soluble than Fe sulfides (greigite, $pK_{sp} = -3.75$; pyrite, $pK_{sp} = -15.4$; Berner, 1984). Generally, Mn pyritization starts after the majority of amorphous Fe oxyhydroxides have already been pyritized (Morse and Luther III, 1999; Otero and Macías, 2003).

Sulfides in marine sediments are produced by sulfate oxidation of organic matter (eq. 2; Kasten and Jørgensen, 2000), but also by anoxic methane oxidation (AMO) by sulfate (eq. 3).

$$2CH_2O + SO_4^{2-} + 2H^+ \rightarrow H_2S + 2H_2CO_3 \quad (2)$$

$$SO_4^{2-} + CH_4 + Ca^{2+} \rightarrow H_2S + CaCO_3 + H_2O \quad (3)$$

High levels of H_2S production due to AMO have been observed in many deep-sea sediments (Sternbeck and Sochlenius, 1997; Snyder et al., 2007; Lim et al., 2011) and, more recently, in the Ria de Vigo (Ramírez-Pérez et al., 2015). In sediments of the Ria de Vigo, both Mn pyritization (this study) and Fe pyritization (Ramírez-Pérez et al., 2020) have been observed to substantially increase with depth and independently of the presence or absence of methane in the deepest portion of the cores (Table 1 and Fig. 2). These results suggest that the sulfidization observed in the deeper sediment layers could mainly be due to sulfide produced by sulfate reduction bacteria rather than to AOM. Moreover, the results of this study reveal that the Mn-pyritic fraction (F5) increases as fraction F4 decreases, i.e., at the expense of Mn associated with crystalline Fe oxyhydroxides (mainly goethite). The behavior of both fractions (F4 and F5) in relation to depth is symmetrical (see Fig. 2). This behavior is clearly seen in Fig. 2, where reduction of crystalline Fe oxyhydroxides occurs once the Mn associated with amorphous iron oxides (fraction F3) has been depleted, indicating that reduction of MnO_2 and poorly crystalline ferric iron forms occurs in the upper centimeters of the sediments, as has been reported for normal sedimentary environments (i.e. those covered by an oxic water layer; Canfield et al., 2005). Moreover, crystalline Fe oxyhydroxides have been consistently observed in strongly reduced sedimentary environments due to their greater stability even in this type of sediments (Van der Zee et al., 2003) or to the passivation effect of Fe^{2+} adsorption (Roden, 2004; Ramírez-Pérez et al., 2020). Hence, the full depletion of Mn associated with F4 and of Fe-goethite (e.g., Ramírez-Pérez et al., 2020) observed below 100 cm depth (Fig. 2) suggests that sediments of the Ria de Vigo are subjected to intense Fe pyritization (and associated Mn), typical of environments with high levels of H_2S production and consistent with AMO (eq. 3), which in turn suggests that the depths covered by the methane field could have formerly reached depths from which it is currently absent.

Additionally, the results of this study for the whole set of analyzed samples showed that the concentrations of Mn associated with fraction F3 (amorphous or poorly crystalline Mn or associated with ferromanganese oxides) constituted one of the main Mn fractions (400–600 nmol g^{-1}), which barely varied with depth, a finding that is inconsistent with the aforementioned depletion of fraction F4 (Fig. 2). Hydroxylamine is considered a weak reducer that is reasonably selective in dissolving amorphous Fe and Mn hydroxides after removal of carbonates, and it does not attack goethite to a significant extent (FeOOH; Tessier et al., 1989; Fortin et al., 1993; Sager, 1992). However, under the redox conditions found in sediments of the Ria de Vigo, Mn oxides are not stable and should have been reduced to Mn^{2+} in the uppermost sediment layer. In other sedimentary environments, the fraction of sediments that can be leached by hydroxylamine-acetic acid has been observed to dominate upper layers and decrease with depth, mainly due to Mn pyritization in deeper layers (Sager, 1992). However, our results show high concentrations of Mn in fraction F3, even in methanogenic environments. A possible explanation for the behavior of fraction F3 could entail that Mn extracted by hydroxylamine (pH ~2) comes mainly from Mn associated with silicates in the clay fraction (e.g., braunite $Mn^{III}_6Mn^{II}O_8SiO_4$; Herndon et al., 2018) or primary minerals such as amphiboles, as suggested by the results obtained from XANES. Despite the high selectivity of hydroxylamine to extract Mn oxides (Sager, 1992), some authors have reported that hydroxylamine can extract small amounts of Al and Si from chlorites or from low degree smectites (Tessier et al., 1979; Sager, 1992). In our case, this process could have been enhanced by carrying out the extraction at 96°C to guarantee the dissolution of Mn associated with poorly crystalline Fe oxyhydroxides (e.g. lepidocrocite), as reported by Fortin et al. (1993). High concentrations of Si subsequently measured in extracts from fraction F3 (26 ± 0.92 μmol g^{-1}) seem to confirm this idea.

Finally, Mn-carbonate (fraction F2) showed high values in the surface sediments that remained relatively constant in depth, with similar values to those observed in the upper layer (Mn-F2: 300–500 nmol g^{-1}; ~20%–45% of the reactive fraction; Fig. 2). These results suggest that the Mn sources for the formation of Mn-carbonate and of Mn-pyrite are different. Mn-carbonate is found only in anoxic sediments located beneath the surface oxic horizon or under oxygenated bottom water conditions (Calvert and Pedersen, 1996; Lenz et al., 2015). In fact, its presence in sediments is used as a proxy of oxic paleoredox conditions (Poulton and Canfield, 2011; Johnson et al., 2013; Reinhard et al., 2013). Hence, our results suggest that Mn-carbonate is formed in the upper centimeters of the sediments of the ria and close to the sediment-water interface, essentially from Mn associated with Fe oxyhydroxides (fraction F3). This fraction is composed of easily reducible Fe/Mn oxides and oxyhydroxides, which are already depleted in the upper few centimeters (<5 cm) of the sediment layer, where microbial reduction of MnO_2 and poorly crystalline Fe is the dominant pathway for organic carbon oxidation, according to eqs. 4 and 5, inhibiting sulfate reduction and methanogenesis in the process (Canfield et al., 2005).

$$CH_2O + 2MnO_2 + 4H^+ \rightarrow 2Mn^{2+} + H_2CO_3 + 2H_2O \quad (4)$$

$$CH_2O + 4FeOOH + 8H^+ \rightarrow 4Fe^{2+} + H_2CO_3 + 6H_2O \quad (5)$$

The absence of sulfides on surficial sediments, along with an increase in alkalinity and Mn^{2+} concentration (reactions 4 and 5; Fig. 4) in interstitial water, can lead to saturation of a "pseudokutnahorite"-type manganoan carbonate mineral in pore water, according to eq. 6 (Calvert and Pedersen, 1996, Lenz et al., 2015).

$$Ca^{2+} + Mn^{2+} + 2CO_3^{2-} \leftarrow\rightarrow CaMn(CO_3)_2 \quad (6)$$

In anoxic environments, Mn^{2+} has been mainly found in association with the calcite fraction (Kiratli and Ergin, 1996), acting as a nucleation site for Mn^{2+} (Herndon et al., 2018) and precipitating as a manganoan carbonate (Mucci, 1988, 2004; Lenz et al., 2014a, Lenz et al., 2014b) that is either of kutnohorite or "pseudokutnohorite" type ($CaMn(CO_3)_2$; Middelburg et al., 1987; Böttcher, 1998, Peckmann et al., 2001) or dolomite-Mn-carbonate (Mucci, 1988). However, rhodocrocite ($MnCO_3$) is the mineral that has been identified in the surface sediments of the Ria de Vigo (Rubio et al., 2000). Mn-carbonate synthesis is the most relevant diagenetic process affecting Mn in surficial suboxic sediments (i.e., very low H_2S concentration; Fig. 4) of the outermost and middle sections of the Ria de Vigo. In the deeper portions of the sediment, Mn-carbonate content remained high, and no significant changes were observed between the surficial and deeper sections of the sediments or among the deep sections of cores with and without the presence of methane (Table 2). These findings are consistent with the fact that

rhodocrocite or mixed Ca/Mn-carbonates are stable even in the presence of high sulfide concentrations (Herndon et al., 2018).

4.2. Scenario 2. Innermost section of the Ria de Vigo: area of intense methanogenic activity throughout the sedimentary column

The innermost section of the Ria de Vigo (Fig. 1) constitutes a particularly singular geochemical environment that is likely unique within the Galician rias, at least according to current knowledge. San Simon Bay is a semienclosed marine environment connected to the rest of the ria by a narrow channel (Rande Strait), and water renewal is therefore limited. It has an area of 19.4 km^2, a length of 8 km, a maximum width of 3.6 km, and an average water depth < 5 m. San Simon Bay is considered an estuary based on its hydrology and sedimentology (Vilas et al., 1995). Its orientation and morphology result in low-energy hydrodynamics. Moreover, the upwelling phenomenon (intrusion of nutrient-rich water) makes San Simon Bay (and the whole Ria de Vigo) a coastal ecosystem of high biological productivity, which in turn results in increased input of organic matter to the seabed (TOC: 7%–10%; Vilas et al., 1995), promoting the development of anoxic-sulfidic conditions in sediments, as well as biogenic methane production (Egger et al., 2016).

In San Simon Bay sediments, methane has been found below 90 cm depth, with concentrations ranging from 0.1 to 0.9 mM (Ramírez-Pérez et al., 2015). However, different authors have observed the emission of methane bubbles to the water column through the formation of pockmarks in sediments (Martínez-Carreño and García-Gil, 2017, among others). These flow events have been associated with sediments with strongly reduced conditions and high H_2S concentrations (Eh < −150 mV; 0.3 and 18.5 mM, respectively; Ramírez-Pérez et al., 2015). These conditions lead to intense Fe pyritization processes throughout the whole sedimentary column (DOP: 66 ± 9%; Ramírez-Pérez et al., 2020), but with very low concentrations of acid volatile sulfide (0.18 ± 0.09 μmol g^{-1}; Ramírez-Pérez et al., 2020). These extreme redox conditions, with Fe-pyritic contents similar to or higher than those observed in euxinic environments, have been related to AMO by sulfate (eq. 3). Under these conditions, not only Fe but also Mn is intensely pyritized (Fig. 2). Few marine environments have shown intense Mn pyritization, with mean values ranging from 44% to 49% (Table 2). Thus, in euxinic environments such as the Baltic Sea, formation of Mn sulfides has been observed (Böttcher and Huckriede, 1997; Lenz et al., 2014a, Lenz et al., 2014b), albeit at lower levels than in this study (Fig. 7). Additionally, high values were observed in deep sediment layers with presence of methane (DTMP-Mn 27%, Table 2). In this case, we consider that the significantly lower pyritization of Mn in deep sediments with the presence of methane is at least partially due to that part of the reactive Mn having previously been "sequestered" as Mn-carbonate, which formed on the surface prior to being buried. The significant negative correlation between Mn-carbonate and Mn-pyrite contents ($r = -0.565$, $p < 0.01$, $n = 12$; Fig. 4) observed in deep samples from cores with methane seems to support this hypothesis.

However, in the case of San Simon Bay (Core8), Mn carbonation does not occur, since the high H_2S production associated with AOM leads to rapid Mn pyritization. Manganese must be incorporated into the pyrite fraction during pyrite formation since, as mentioned above, the formation of a pure MnS phase is extremely rare (e.g., Böttcher and Huckriede, 1997; Lenz et al., 2014a, Lenz et al., 2014b). The identification of Mn—S bonds in the EXAFS observed on core8 but not in core11 and core10, together with the highly significant correlation between DOP and DTMP-Mn in the innermost section of the ria (C8-GI), seem to support this idea ($r = 0.83$, $p < 0.001$). Finally, the fact that DTMP-Mn values did not exceed 60% is consistent with the aforementioned fact that part of the Mn extracted in F3 corresponds to a recalcitrant fraction such as silicates (Canfield, 1989), leading to an overestimation of the reactive fraction and, thus, to a decrease in the value of DTMP-Mn.

5. Conclusions

Two geochemical scenarios with sharp differences have been identified. One of them corresponds to San Simon Bay, located in the innermost section of the Ria de Vigo, where the high organic matter content present in the sediment, promoted by mussel farming and restricted water circulation, leads to highly reduced conditions and high production of methane, which diffuses throughout the sediment column until it reaches the sediment-water interface. This diffusion process promotes anaerobic oxidation of sulfate, with the subsequent generation

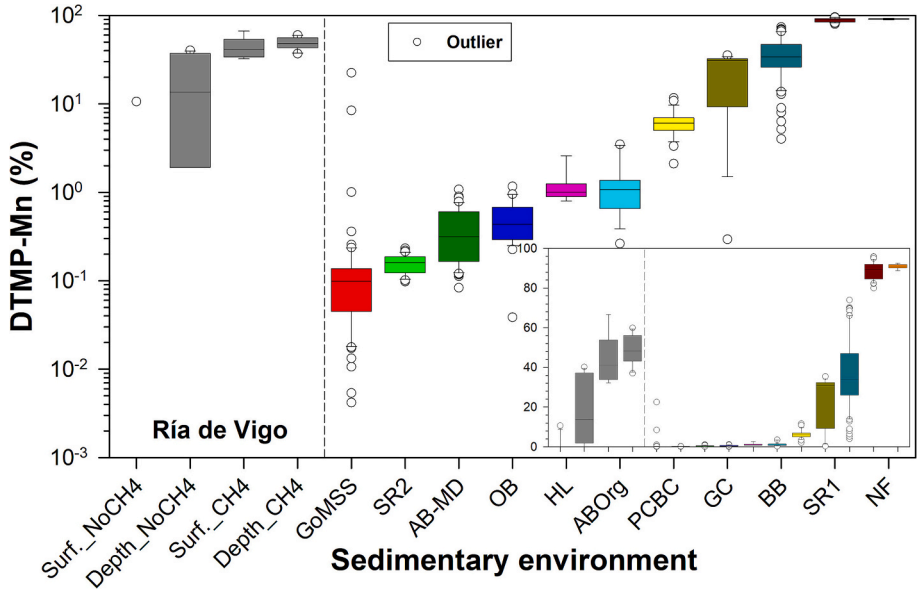

Fig. 7. Degrees of trace metal pyritization of manganese (DTMP-Mn) in sediments of the Ria de Vigo and other marine environments: Gulf of Mexico shelf and slope (GoMSS), Atchafalaya Bay-Mississippi Delta (AB-MD), Orca Basin (OB), organic-rich Atchafalaya Bay (ABOrg), Green Canyon (GC), Baffin Bay, Texas (BB) (Huerta-Diaz and Morse, 1992), Santa Rosalia, Baja California (SR1, SR2; Huerta-Diaz et al., 2014), Haringvliet Lake, Netherlands (HL; Canavan et al., 2007), Nordåsvannet Fjord, Norway (NF; Müller A., 2002), and Pacific Coast of Baja California (PCBC; Nava-López and Huerta-Díaz, 2001). (For interpretation of the references to colour in this figure legend, the reader is referred to the web version of this article.)

of H_2S and intense Mn pyritization throughout the sediment column, a process similar to those observed in euxinic environments.

The second scenario corresponds to the rest of the Ria de Vigo (middle and outermost sections), where the dominant Mn fraction is Mn-carbonate, even at depth within the sediment and in the presence of methane, where the concentration of this fraction is comparable to that of Mn-pyrite. The concentrations of the remaining geochemical fractions are virtually negligible, except for the forms associated with Fe oxyhydroxides or the easily reducible forms found in the upper centimeters of the sediment column. It is worth pointing out that extraction with hydroxylamine at high temperature (e.g., 96°C) seems to extract significant amounts of silicate-associated Mn, leading to an underestimation of DTMP-Mn.

Finally, the hydrodynamic, morphological, and geochemical conditions in the Ria de Vigo constitute an excellent scenario for the study of biogeochemical processes in marine sedimentary environments regulating the mobility and bioavailability of metals and nutrients, such as P, which have been poorly studied.

Data in this study are publicly available at https://data.mendeley.com/datasets/wvym957mwp/1

CRediT authorship contribution statement

X.L. Otero: Conceptualization, Funding acquisition, Methodology, Supervision, Writing – original draft, Writing – review & editing. **A.M. Ramírez-Pérez:** Conceptualization, Formal analysis, Investigation, Methodology, Writing – original draft, Writing – review & editing. **M. Abernathy:** Formal analysis, Investigation, Writing – original draft, Writing – review & editing. **S.C. Ying:** Formal analysis, Funding acquisition, Methodology, Supervision, Writing – original draft, Writing – review & editing. **H.M. Queiroz:** Formal analysis, Investigation, Writing – original draft, Writing – review & editing. **T.O. Ferreira:** Conceptualization, Formal analysis, Investigation, Writing – original draft, Writing – review & editing. **M.A. Huerta-Díaz:** Conceptualization, Formal analysis, Investigation, Supervision, Visualization, Writing – original draft, Writing – review & editing. **E. de Blas:** Conceptualization, Formal analysis, Investigation, Writing – original draft, Writing – review & editing.

Declaration of Competing Interest

The authors declare the following financial interests/personal relationships which may be considered as potential competing interests:

Xose Luis Otero reports financial support was provided by Government of Galicia Department of Culture Education and Universities. Analysis in the Stanford Synchrotron Radiation Lightsource were supported by the U.S. Department of Energy, Office of Science, Office of Basic Energy Sciences under Contract No. DE-AC02-76SF00515.

Acknowlegments

This research was co-funded by the Spanish Ministry of Economy and Competitiveness (CGL2012–33584) and the Consellería de Educación, Universidade e Formación Profesional-Xunta de Galicia (Axudas á consolidación e estruturación de unidades de investigación competitivas do SUG do Plan Galego IDT, Ambiosol Group ref. ED431C 2022/40). Thanks are due to María José Santiso for her assistance with laboratory work. The use of the Stanford Synchrotron Radiation Lightsource, SLAC National Accelerator Laboratory, was supported by the U.S. Department of Energy, Office of Science, Office of Basic Energy Sciences under Contract No. DE-AC02-76SF00515.

Appendix A. Supplementary data

Supplementary data to this article can be found online at https://doi.org/10.1016/j.margeo.2024.107250.

References

Aller, R.C., 1980. Quantifying solute distributions in the bioturbated zone of marine sediments by defining an average microenvironment. Geochim. et Cosmochim. Acta 44, 1955–1965.
Alvarez, M., Sileo, E.E., Rueda, E.H., 2005. Effect of Mn(II) incorporation on the transformation of ferrihydrite to goethite. Chem. Geol. 216, 89–97.
Álvarez-Salgado, X.A., Gago, J., Míguez, B.M., Gilcoto, M., Pérez, F.F., 2000. Surface waters of the NW Iberian margin: upwelling on the shelf versus outwelling of upwelled waters from the Rías Baixas. Estuar. Coast. Shelf Sci. 51, 821–837.
Beal, E.J., House, C.H., Orphan, V.J., 2009. Manganese- and iron-dependent marine methane oxidation. Science 325, 184–187.
Belzunce-Segarra, M.J., Wilson, M.J., Fraser, A.R., Lachowski, E., Duthie, D.M.L., 2002. Clay mineralogy of Galician Coastal and oceanic surface sediments: contributions from terrigenous and authigenic sources. Clay Miner. 37, 23–37.
Berner, R.A., 1984. C/S method for distinguishing freshwater from marine sedimentary rocks. Geology 12, 365–368.
Böttcher, M.E., 1998. Manganese(II) partitioning during experimental precipitation of rhodochrosite-calcite solid solutions from aqueous solutions. Mar. Chem. 62, 287–297. https://doi.org/10.1180/0009855023710015.
Böttcher, M.E., Huckriede, H., 1997. First occurrence and stable isotope composition of authigenic γ-MnS in the Central Gotland deep (Baltic Sea). Mar. Geol. 137, 201.
Brookins, D.G., 1988. Eh-pH Diagrams for Geochemistry, 1st ed. Springer-Verlag, Berlin Heidelberg. https://doi.org/10.1007/978-3-642-73093-1.
Burdige, D.J., 1993. The biogeochemistry of manganese and iron reduction in marine sediments. Earth Sci. Rev. 35, 249–284.
Calvert, S.E., Pedersen, T.F., 1993. Geochemistry of recent oxic and anoxic marine sediments: implications for the geological record. Mar. Geol. 113, 67–88.
Calvert, S., Pedersen, T., 1996. Sedimentary geochemistry of manganese; implications for the environment of formation of manganiferous black shales. Econ. Geol. 91 (1), 36–47.
Canavan, R.W., Van Cappellen, P., Zwolsman, J.J.G., van den Berg, G.A., Slomp, C.P., 2007. Geochemistry of trace metals in a freshwater sediment: Field results and diagenetic modeling. Sci. Total Environ. 381, 263–279.
Canfield, D.E., 1989. Reactive iron in marine sediments. Geochim. Cosmochim. Acta 53, 619–632.
Canfield, D.E., Kristensen, E., Thamdrup, B., 2005. Aquatic Geomicrobiology. Academic Press.
Chalmin, E., Farges, F., Brown, G.E., 2009. A pre-edge analysis of Mn K-Edge XANES Spectra to help determine the speciation of manganese in minerals and glasses. Contrib. Mineral. Petrol. 157 (1), 111–126. https://doi.org/10.1007/s00410-008-0323-z.
Egger, M., Rasigraf, O., Sapart, C.J., Jilbert, T., Jetten, M.S.M., Röckmann, T., Van Der Veen, C., Bânda, N., Kartal, B., Ettwig, K.F., Slomp, C.P., 2015. Iron-mediated anaerobic oxidation of methane in brackish coastal sediments. Environ. Sci. Technol. 49, 277–283.
Della Ventura, G., Robert, J.L., Raudsep, P.M., Hawthorne, F.C., 1993. Site occupancies inmonoclinic amphiboles: Rietveld structure refinement of synthetic nickel magnesium cobalt potassium richterite. Amer. Mineral. 78, 633–640.
Egger, M., Lenstra, W., Jong, D., Meysman, F.J.R., Sapart, C.J., van der Veen, C., et al., 2016. Rapid sediment accumulation results in high methane effluxes from coastal sediments. PloS One 11 (8). https://doi.org/10.1371/journal.pone.0161609 e0161609.
Elderfield, H., 1981. Metal-organic associations in interstitial waters of Narragansett Bay sediments. Am. J. Sci. Nov. 1981 281 (9), 1184–1196. https://doi.org/10.2475/ajs.281.9.1184.
Ettwig, K.F., Zhu, B., Speth, D., Keltjens, J.T., Jetten, M.S.M., Kartal, B., 2016. Archaea catalyze iron-dependent anaerobic oxidation of methane. Proc. Natl. Acad. Sci. USA 113, 12792–12796.
Ferrín, A., Durán, R., Diez, R., García-Gil, S., Vilas, F., 2003. Shallow gas features in the Galician Rias Baixas (NW Spain). Geo-Mar. Lett. 23, 207–214.
Figueiras, F.G., Labarta, U., Fernádez Reíriz, M.J., 2002. Coastal Upwelling, Primary Production and Mussel Growth in the Rías Baixas of Galicia. Hydrobiologia 484, 121–131.
Fortin, D., Leppard, G.G., Tessier, A., 1993. Characteristics of lacustrine diagenetic iron oxyhydroxides. Geochim. Cosmochim. Acta 57, 4391–4404.
García-García, A., García-Gil, S., Vilas, F., 2005. Quaternary evolution of the Ría de Vigo, Spain. Mar. Geol. 220, 153–179.
García-Gil, S., de Blas, E., Martínez-Carreño, N., Iglesias, J., Rial-Otero, R., Simal-Gándara, J., Judd, A.G., 2011. Characterization and preliminary quantification of the methane reservoir in a coastal sedimentary source: San Simón Bay, ría de Vigo, NW Spain. Estuar. Coast. Shelf Sci. 91, 232–242.
García-Gil, S., Cartelle, V., De Blas, E., De Carlos, A., Díez, R., Durán, R., Ferrín, A., García-Moreiras, I., García-García, A., Iglesias, J., Martínez-Carreño, N., Muñoz Sobrino, C., Ramírez-Pérez, A.M., 2015. Shallow gas in the Iberian continental margin. Bol. Geol. Miner. 126, 575–608.
Guevara, P. 2020. Variabilidad espacio-temporal de la concentración de metales traza en suelos y sedimentos en la Ría de Ortigueira en relación con las fuentes y dinámica resiudal de las corrientes marinas. PhD Thesis Santiago de Compostela University.
Glasby, G.P., 1984. Manganese in the marine environment. Oceanography and Marine Biology an Annual Review 22, 169–194.
Herndon, E.M., Havig, J.R., Singer, D.M., McCormick, M.L., Kump, L.R., 2018. Manganese and iron geochemistry in sediments underlying the redox-stratified Fayetteville Green Lake. Geochim. Cosmochim. Acta 231, 50–63.

Holmkvist, L., Ferdelman, T.G., Jørgensen, B.B., 2011a. A cryptic sulfur cycle driven by iron in the methane zone of marine sediment (Aarhus Bay, Denmark). Geochim. Cosmochim. Acta 75, 3581–3599.
Holmkvist, L., Kamyshny, A., Vogt, C., Vamvakopoulos, K., Ferdelman, T.G., Jørgensen, B.B., 2011b. Sulfate reduction below the sulfate-methane transition in Black Sea sediments. Deep-Sea Res. Part I Oceanogr. Res. Pap. 58, 493–504.
Holtstam, D., Cámara, F., Skogby, H., Karlsson, A., Langhof, J., 2019. Description and recognition of potassic-richterite, an amphibole supergroup mineral from the Pajsberg Ore Field, Värmland, Sweden. Mineral. Petrol. 113 (1), 7–16. https://doi.org/10.1007/s00710-018-0623-6.
Howarth, R., Evans, G., Croudace, I., Cundy, A., 2005. Sources and timing of anthropogenic pollution in the Ensenada de San Simón (Inner Ría de Vigo), Galicia, NW Spain: an application of mixture-modelling and nonlinear optimization to recent sedimentation. Sci. Total Environ. 340 (1–3), 149–176. https://doi.org/10.1016/j.scitotenv.2004.08.001.
Huerta-Diaz, M.A., 1989. Geochemistry of trace metals associated with sedimentary pyrite from anoxic marine environments. Ph.D. Texas A&M University, pp. 299–p.
Huerta-Diaz, M.A., Morse, J.W., 1990. A quantitative method for determination of trace metal concentrations in sedimentary pyrite. Mar. Chem. 29, 119–144.
Huerta-Diaz, M.A., Morse, J.W., 1992. Pyritization of trace metals in anoxic marine sediments. Geochim. Cosmochim. Acta 56, 2681–2702.
Huerta-Diaz, M.A., Muñoz-Barbosa, A., Otero, X.L., Valdivieso-Ojeda, J., Amaro-Franco, E.C., 2014. High variability in geochemical partitioning of iron, manganese and harmful trace metals in sediments of the mining port of Santa Rosalia, Baja California Sur, Mexico. J. Geochem. Explor. 145, 51–63.
Iglesias, J., Garcia-San Gil, S., 2007. High-resolution mapping of shallow gas accumulations and gas seeps in San Simón Bay (Ría de Vigo, NW Spain). Some quantitative data. Geo-Mar. Lett. 2007 (27), 103–114.
Johnson, J.E., Webb, S.M., Thomas, K., Ono, S., Kirschvink, J.L., Fischer, W.W., 2013. Manganese-oxidizing photosynthesis before the rise of cyanobacteria. Proc. Natl. Acad. Sci. 110, 11238–112.
Kasten, S., Jørgensen, B.B., 2000. Sulfate reduction in marine sediments. In: Schulz, H.D., Zabel, M. (Eds.), Marine Geochemistry. Springer, Berlin, pp. 263–282.
Kiratli, N., Ergin, M., 1996. Partitioning of heavy metals in surface Black Sea sediments. Appl. Geochem. 11, 775–788.
Lenz, C., Behrends, T., Jilbert, T., Silveira, M., Slomp, C.P., 2014a. Redox-dependent changes in manganese speciation in Baltic Sea sediments from the holocene thermal maximum: an EXAFS, XANES and LA-ICP-MS study. Chem. Geol. 370, 49–57. https://doi.org/10.1016/j.chemgeo.2014.01.013.
Lenz, C., Behrends, T., Jilbert, T., Silveira, M., Slomp, C., 2014b. Redox-dependent changes in manganese speciation in Baltic Sea sediments from the Holocene thermal Maximum: an EXAFS, XANES and LA-ICP-MS study. Mar. Geol. 370, 49–57.
Lenz, C., Jilbert, T., Conley, D.J., 2015. Hypoxia-driven variations in iron and manganese shuttling in the Baltic Sea over the past 8 kyr. Geochem. Geophys. Geosyst. 16, 3754–3766. https://doi.org/10.1002/2015GC005960.
Lepland, A., Stevens, R.L., 1998. Manganese authigenesis in the Landsort Deep, Baltic Sea. Marine Geol. 151, 1–25.
Leu, A.O., Cai, C., McIlroy, S.J., et al., 2020. Anaerobic methane oxidation coupled to manganese reduction by members of the *Methanoperedenaceae*. ISME J 14, 1030–1041. https://doi.org/10.1038/s41396-020-0590-x.
Lim, Y.C., Lin, S., Yang, T.F., Chen, Y.-G., Liu, C.-S., 2011. (2011) Variations of methane induced pyrite formation in the accretionary wedge sediments offshore southwestern Taiwan. Mar. Pet. Geol. 28, 1829–1837.
Manceau, A., Marcus, M.A., Grangeon, S., 2012. Determination of Mn valence states in mixed-valent manganates by XANES spectroscopy. Am. Mineral. 97 (5–6), 816–827. https://doi.org/10.2138/am.2012.3903.
Martínez-Carreño, N., García-Gil, S., 2013. The Holocene gas system of the Ría de Vigo (NW Spain): Factors controlling the location of gas accumulations, seeps and pockmarks. Mar. Geol. 344, 1–19.
Martínez-Carreño, N., García-Gil, S., 2017. Reinterpretation of the quaternary sedimentary infill of the Ría de Vigo, NW Iberian Peninsula, as a compound incised valley. Quat. Sci. Rev. 173, 124–144.
Middelburg, J.J., De Lange, G.J., Van der Weijden, C.H., 1987. Manganese solubility control in marine pore waters. Geochim. Cosmochim. Acta 51, 759–763.
Morse, J.W., Luther III, G.W., 1999. Chemical influences on trace metal-sulfide interactions in anoxic sediments. Geochim. Cosmochim. Acta 63, 3373–3378.
Mucci, A., 1988. Manganese uptake during calcite precipitation from seawater: conditions leading to the formation of a pseudokutnahorite. Geochim. Cosmochim. Acta 52, 1859–1868.
Mucci, A., 2004. The behavior of mixed Ca-Mn carbonates in water and seawater: controls of manganese concentrations in marine porewaters. Aquat. Geochem. 10, 139–169.
Myhre, G., D. Shindell, F.-M. Bréon, W. Collins, J. Fuglestvedt, J. Huang, D. Koch, J.-F. Lamarque, D. Lee, B. Mendoza, T. Nakajima, A. Robock, G. Stephens, T. Takemura, and H. Zhang, 2013. Anthropogenic and natural radiative forcing. In Climate Change 2013: The Physical Science Basis. Contribution of Working Group I to the Fifth Assessment Report of the Intergovernmental Panel on Climate Change. T.F. Stocker, D. Qin, G.-K. Plattner, M. Tignor, S.K. Allen, J. Doschung, A. Nauels, Y. Xia, V. Bex, and P.M. Midgley, Eds., Cambridge University Press, pp. 659-740,doi:10.1017/CBO9781107415324.018.
Macías, F., Mora, J. 2001. Biogeochemical processes and benthic communities in the bottom sediments under mussel rafts in the Rias of Galicia, Xunta de Galicia, Unpublished Report.
Newville, M., 2013. Larch. J. Phys. Conf. Ser. 430 https://doi.org/10.1088/1742-6596/430/1/012007, 012007.
Oberti, R., Vannucci, R., Zanetti, A., Tiepolo, M., Brumm, R.C., 2000. A crystal chemical re-evaluation of amphibole/melt and amphibole/clinopyroxene D Ti values in petrogenetic studies. Am. Mineral. 85 (3–4), 407–419. https://doi.org/10.2138/am-2000-0402.
Otero, X.L., Macías, F., 2003. Spatial variation in pyritization of trace metals in salt marsh soils. Biogeochemistry 62, 59–86.
Otero, X.L., Huerta-Díaz, M.A., Macías, F., 2003. Influence of a turbidite deposit on the extent of pyritization of iron, manganese and trace metals in sediments from the Guaymas Basin, Basin of California (Mexico). Appl. Geochem. 18, 1149e1163.
Otero, X.L., Vidal-Torrado, P., Calvo De Anta, R.M., Macías, F., 2005. Trace elements in biodeposits and sediments from mussel culture in the ría de arousa (Galicia, NW Spain). Environ. Pollut. 136 (1), 119–134.
Otero, X.L., Calvo De Anta, R.M., Macías, F., 2006. Sulphur partitioning in sediments and biodeposits below mussel rafts in the Ría de Arousa (Galicia, NW Spain). Mar. Environ. Res. 61, 305–325.
Otero, X.L., Ferreira, T.O., Huerta-Díaz, M.A., Partiti, C.S.M., Souza Jr., V., Vidal-Torrado, P., Macías, F., 2009. Geochemistry of iron and manganese in soils and sediments of a mangrove system, Island of Pai Matos (Cananeia - SP, Brazil). Geoderma 148, 318–335.
Pais, J., Jones, J.B., 1997. The Handbook of Trace Elements. CRC Press, Boca Raton.
Peckmann, J., Reimer, A., Luth, U., Luth, C., Hansen, B.T., Heinicke, C., Hoefs, J., Reitner, J., 2001. Methane-derived carbonates and authigenic pyrite from the northwestern Black Sea. Mar. Geol. 177, 129–150.
Poulton, S.W., Canfield, D.E., 2011. Ferruginous conditions: a dominant feature of the ocean through Earth's history. Elements 7, 107–112.
Poulton, S.W., Raiswell, R., 2000. Solid phase associations, oceanic fluxes and the anthropogenic perturbation of transition metals in world river particulates. Marine Chem. 72, 17–31.
Prego, R., 1993. General aspects of carbon biogeochemistry in the ria of Vigo, northwestern Spain. Geochim. Cosmochim. Acta 57, 2041–2052.
Ramírez-Pérez, A.M., de Blas, E., García-Gil, S., 2015. Redox processes in pore water of anoxic sediments with shallow gas. Sci. Total Environ. 538, 317–326.
Ramírez-Pérez, A.M., de Blas, E., García-Gil, S., 2017. Sulfur, Iron, and manganese speciation in anoxic sediments with methane (Ría de Vigo, NW Spain). Clean Soil Air Water 45,1600700.
Ramírez-Pérez, A.M., de Blas, E., Otero, X.L., 2020. Iron pyritization in shallow methane fields in sediments of the ría de Vigo (NW Iberian Peninsula). Estuar. Coast. Shelf Sci. 235.
Ravel, B., Newville, M., 2005. ATHENA, ARTEMIS, HEPHAESTUS: data analysis for X-ray absorption spectroscopy using IFEFFIT. J. Synchrotron Radiat. 12 (4), 537–541. https://doi.org/10.1107/S0909049505012719.
Reinhard, C.T., Planavsky, N.J., Robbins, L.J., Partin, C.A., Gill, B.C., Lalonde, S.V., Bekker, A., Konhauser, K.O., Lyons, T.W., 2013. Proterozoic ocean redox and biogeochemical stasis. Proc. Natl. Acad. Sci. 110, 5357–5362.
Robie, R.A., 1966. Thermodynamic properties of minerals. Mem. Am. Geol. Soc. 97, 437–458.
Roden, E.E., 2004. Analysis of long-term bacterial vs. chemical Fe(III) oxide reduction kinetics. Geochem. Cosmochim. Acta 68, 3205–3216.
Rubio, B., Nombela, M., Vilas, F., 2000. Geochemistry of major and trace elements in sediments of the ria de Vigo (NW Spain): an assessment of metal pollution. Mar. Pollut. Bull. 40, 968–980.
Russell, A.D., Morford, J.L., 2001. The behavior of redox-sensitive metals across a laminated–massive–laminated transition in Saanich Inlet, British Columbia. Mar. Geol. 174 (1–4), 341–354.
Sager, M., 1992. Chemical speciation and environmental mobility of heavy metals in sediments and soils. In: Stoeppler, M. (Ed.), Hazardous Metals in the Environment. Elsevier, pp. 132–175. Chapter 7.
Santelli, C.M., Webb, S.M., Dohnalkova, A.C., Hansel, C.M., 2011. Diversity of Mn oxidesproduced by Mn(II)-oxidizing fungi. Geochem. Cosmochim. Acta 75, 2762–2776. https://doi.org/10.1016/j.gca.2011.02.022.
Segarra, M.J.B., Prego, R., Wilson, M.J., Bacon, J., Santos-Echeandía, J., 2008. Metal speciation in surface sediments of the Vigo Ria (NW Iberian Peninsula). Sci. Mar. 8.
Segarra, K.E.A., Comerford, C., Slaughter, J., Joye, S.B., 2013. Impact of electron acceptor availability on the anaerobic oxidation of methane in coastal freshwater and brackish wetland sediments. Geochim. Cosmochim. Acta 115, 15–30.
Sivan, O., Adler, M., Pearson, A., Gelman, F., Bar-Or, I., John, S.G., Eckerte, W., 2011. Geochemical evidence for iron-mediated anaerobic oxidation of methane. Limnol. Oceanograph. 56 https://doi.org/10.4319/lo.2011.56.4.1536.
Snyder, G.T., Hiruta, A., Matsumoto, R., Dickens, G.R., Tomaru, H., Takeuchi, R., Komatsubara, J., Ishida, Y., Yu, H., 2007. Pore water profiles and authigenic mineralization in shallow marine sediments above the methane charged system on Umitaka Spur, Japan Sea. Deep Sea Res. 54, 1216e1239.
Souto, C., Gilcoto, M., Fariña-Busto, L., Pérez, F.F., 2003. Modelling the residual circulation of coastal embayment affected by wind-driven upwelling: circulation of the Ría de Vigo (NW Spain). J. Geophys. Res. 108, 1–18.
Sternbeck, J., Sochlenius, G., 1997. Authigenic sulfide and carbonate mineral formation in Holocene sediments of the Baltic Sea. Chem. Geol. 135, 55–73.
Suess, E., 1979. Mineral phases formed in anoxic sediments by microbial decomposition of organic matter. Geochim. et Cosmochim. Acta 43, 339–352.
Sundby Bjørn, Silverberg, Norman., 1985. Manganese fluxes in the benthic boundary layer. Limnol. Oceanograph. 2 https://doi.org/10.4319/lo.1985.30.2.0372.
Tenore, K.R., Alonso-Noval, M., Alvarez-Ossorio, M., Atkinson, L.P., Cabanas, J.M., Cal, R.M., Campos, H.J., Castillejo, F., Chesney, E.J., Gonzalez, N., Hanson, R.B., McClain, C.R., Miranda, A., Roman, M.R., Sanchez, J., Santiago, G., Valdes, L., Varela, M., Yoder, J., 1995. Fisheries and oceanography off Galicia, NW Spain:

mesoscale spatial and temporal changes in physical processes and resultant patterns of biological productivity. J. Geophys. Res. Oceans 100, 10,943–10,966.
Tessier, A., Campbell, P.G.C., Bisson, M., 1979. Sequential extraction procedure for the speciation of particulate trace metals. Anal. Chem. 51, 844–851.
Tessier, A., Carignan, R., Dubbreuil, B., Rapin, F. 1989 Iron behavior in a northern estuary: large pools of non-sulfidized Fe(II) associated with organic matter.
Thamdrup, B., Fossing, H., Jørgensen, B.B., 1994. Manganese, iron, and sulfur cycling in a coastal marine sediment, Aarhus Bay, Denmark. Geochim. Cosmochim. Acta 58, 5115–5129. https://doi.org/10.1016/0016-7037(94)90298-4.
Torres López, S., Varela, R.A., Delhez, E., 2001. Residual circulation and thermohaline distribution of the Ría de Vigo: A 3-D hydrodynamical model. Sci. Mar. 65, 277–289.
Van der Zee, C., Roberts, D.G., Rancourt, D.G., Slomp, C.P., 2003. Nanogoethite is the dominant reactive oxyhydroxide phase in lake and marine sediments. Geology 31, 993–996.
Vilas, F., 2002. Coastal zones and estuaries. In: Rías and Tidal-Sea Estuaries. Unesco-EOLSS.
Vilas, F., Nombela, M.A., Garcia-Gil, E., García-Gil, S., Alejo, I., Rubio, B., Pazos, O., 1995. Mapa de distribución de los sedimentos del fondo de la Ría de Vigo. Consellería de Pesca, Marisqueo y Acuicultura, Xunta de Galicia.
Welch, M.D., 2021. Amphiboles. In: Alderton, D., Elias, S.A. (Eds.), Encyclopedia of Geology, Second edition. Academic Press, Oxford, pp. 297–300. https://doi.org/10.1016/B978-0-08-102908-4.00095-3.
Yu, C., Virtasalo, J.J., Karlsson, T., Peltola, P., Österholm, P., Burton, E.D., Arppe, L., Hogmalm, J.K., Ojala, A.E.K., Åström, M.E., 2015. Iron behavior in a northern estuary: large pools of non-sulfidized Fe(II) associated with organic matter. Chem. Geol. 413, 73–85.